Scratch Toughness of Viscoelastic Liquids

Asheesh Shukla,[1] Nicolas Chanut,[2] Roland J.-M. Pellenq,[1,2,3] Thibaut Divoux,[2,4] and Franz-Josef Ulm[1,2,*]

[1] *Department of Civil and Environmental Engineering, Massachusetts Institute of Technology, Cambridge MA 02139, USA*
[2] *MIT–CNRS–AMU Joint Laboratory, Massachusetts Institute of Technology, Cambridge MA 02139, USA*
[3] *Department of Physics, Georgetown University, Washington DC 20057, USA*
[4] *Univ Lyon, Ens de Lyon, Univ Claude Bernard, CNRS, Laboratoire de Physique, F-69342 Lyon, France*

(Dated: March 1, 2021)

We present results of a hybrid experimental-theoretical investigation of the scratch resistance of viscoelastic liquids, in which rate-dependent viscous dissipation competes with instantaneous fracture energy dissipation for stored elastic energy. We find that the stationary nature of the scratch test permits separating rate effects from rate-independent fracture properties. We rationalize experimental observations in the form of an analytical model that considers a moving reference system and a characteristic viscous fracture length attached to the crack front, along which viscous deformation is captured by a fractional model. The predictive power of the model is illustrated for highly viscous colloidal suspensions of bitumen and validated by independent rheological measurements. The results extend the realm of the scratch technique, well-entrenched for material characterization of 'hard' materials, to 'soft' materials with the same level of high fidelity.

PACS numbers:

The fracture behavior of soft matter is a highly topical research field in experimental mechanics, not least because of its practical implications for many soft matter materials' applications, ranging from viscoelastic solids, e.g., hydrogels and elastomers [1–3] to viscoelastic liquids, e.g., micellar solutions [4], microemulsions bridged by polymers [5, 6], and soft bitumens, the binder phase of asphalt in our road infrastructure systems [7]. In particular, viscoelastic liquids exhibit a large range of viscous relaxation times, which entails large viscous deformation prior to fracture, stress relaxation in the fracture process zone, and crack tip blunting that affect stress singularities in the fracture process zone leading to rate effects [8–10]. Consequently, fracture propagation becomes challenging to follow experimentally or intractable [11]. This has been a major obstacle to quantitatively assessing intrinsic time-independent fracture properties of soft materials (e.g., hydrogels, rubbers, etc.) through classical fracture tests, such as pure shear and simple extension tests [12], single edge crack tests [13], tearing tests [14]; or advanced cutting tests such as the single notch knife test [15], which all exhibit pronounced rate effects in the fracture response. Although more advanced test methods such as cavitation experiments, in which a liquid is injected via a syringe into hydrogels, have provided an indirect means to monitor via the pressure response of the swollen polymer the occurrence and scaling of cavitation [16, 17], to the best of our knowledge none of these tests provides a means to unambiguously separate rate effects related to viscous deformation from fracture resistance.

Here, we focus on energy dissipation mechanisms in stationary fracture propagation in scratching of viscoelastic liquids. Illustrated for highly viscous colloidal suspensions of bitumen [Fig. 1(a)], we approach the problem through a combination of experiments and first-order modeling. In both experiments and theory, we show that the deliberate choice to describe energy changes in terms of a reference system attached to the moving crack front, provides a quantitative means to systematically separate rate effects from rate-independent fracture behavior in soft materials.

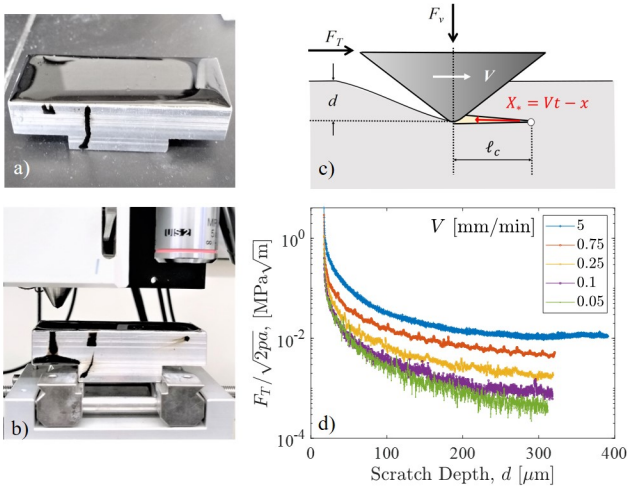

FIG. 1: (a) Bitumen, a viscoelastic liquid, which cannot hold its shape at ambient temperature, is poured at 150°C into an aluminum mold (of 625 mm length) to obtain a smooth surface, and cooled to ambient temperature for use in (b) an instrumented scratch equipment (Micro Combi Tester, Anton Paar). (c) In the scratch test, a constant vertical loading rate $\dot{F}_v$ and scratch speed V are applied, and the scratch depth d and tangential force F_T are recorded. Also shown is the moving coordinate system, $X_* = Vt - x$, attached to the crack tip at a distance ℓ_c from the scratch probe. (d) Convergence of the scratch toughness $K_s = \lim_d (F_T/\sqrt{2pA})$ with increasing scratch depth to a horizontal asymptote for bitumen 35/50 tested at $\dot{F}_v = 0.02$ N/min, and different scratch speeds V.

The fracture test we here consider is the instrumented scratch test originally devised for 'hard' brittle materials [18] [Fig. 1(b-c)]: a sample is clamped on a stage, which moves with a constant speed V, while being simultaneously subject to a vertical loading rate $\dot{F}_v$, transmitted through an almost rigid scratch probe. In the scratch test, the scratch force F_T, and the scratch depth d, are recorded. Known for its versatility and unique scaling with scratch depth [18], scratch speed and loading rates [19, 20], these measurements provide not only a means to discriminate fracture response from stress-driven bulk deformation mechanisms [3, 21, 22]. Herein we argue that the scratch test is an ideal tool for investigating stationary crack propagation in soft matter, in that (i) the surface fracture propagation at the material–probe interface is highly controlled by the prescribed scratch speed, minimizing the influence of inertia effects and (uncontrolled) fracture burst events throughout the test; and (ii) seen from the scratch probe, which provides external work to the system, energy changes occur in a moving coordinate system, $X_* = Vt - x$, along the scratch path, x, over scratch time t [Fig. 1(c)]. This choice of a moving reference system will turn out key for rationalizing rate effects in the scratch-fracture response.

We start by measuring the scratch toughness of a set of bitumen samples of different hardness. The tests are carried out at room temperature, i.e., well above the glass transition temperature of bitumen [23]. The bitumen herein considered ranges from hard to soft, as expressed by the penetration grade (PEN-grade), 35/50, 50/70, and 70/100, a standardized min-max penetration depth in units of mm of a 100 g needle in 5 s into a bitumen sample [24]. Set within the framework of stationary crack propagation theory [25, 26], our experimental investigation departs from considering that (i) the measurable 'static' energy release rate, $\mathcal{G}_s$, is amplified by a crack speed function, $\mathcal{F}(V)$, during fracture propagation, for which (ii) the energy release rate equals the rate-independent fracture energy, $\mathcal{G}_s(V)\mathcal{F}(V) = \mathcal{G}_c^0$. Using Irwin's formula [27], $\mathcal{G}_s = K_s^2/E_0$ (where E_0 is the instantaneous elasticity modulus activated in the scratch test), the scratch test permits a direct measurement of the scratch toughness K_s, defined as [18, 21]:

$$K_s(V) = \frac{F_T}{\sqrt{2pA}} = \frac{K_c^0}{\sqrt{\mathcal{F}(V)}} \qquad (1)$$

where $K_c^0 = \sqrt{E_0 \mathcal{G}_c^0}$ is the rate-independent fracture toughness; and $2pA$ the tip area function, a purely geometric function calibrated for a probe type (here, a Rockwell tip, i.e., a cone of opening angle $\theta = 120°$ ending in a hemispherical tip of radius $R = 200$ μm) and reference material (here Lexan, an amorphous polycarbonate), that synthesizes probe perimeter, $p(d)$, and projected contact area, $A(d)$, in function of only the scratch depth, d (for details see Supplemental Material (S.M) [28], which cites Refs. [29, 30]). By way of example, Fig. 1(d) displays for different scratch speeds, V, and a fixed loading rate, $\dot{F}_v = 0.02$N/min, the convergence of the measured scratch toughness of a bitumen sample with increasing scratch depth d to a horizontal asymptote, the converged scratch toughness, $K_s(V)$. For the three bitumen samples considered, Fig. 2(a) displays the experimentally converged scratch toughness K_s vs. the scratch speed V over five orders of magnitude for loading rates varying over two orders of magnitude, $\dot{F}_v \in [0.02, 2]$ N/min. Of interest is the observation that the scratch toughness increases as a power-law of the scratch speed over 4-5 orders of magnitudes, before saturating to an asymptotic value, as predicted by stationary crack propagation theory [i.e., Eq. (1)]. In return, the rate dependence of the fracture

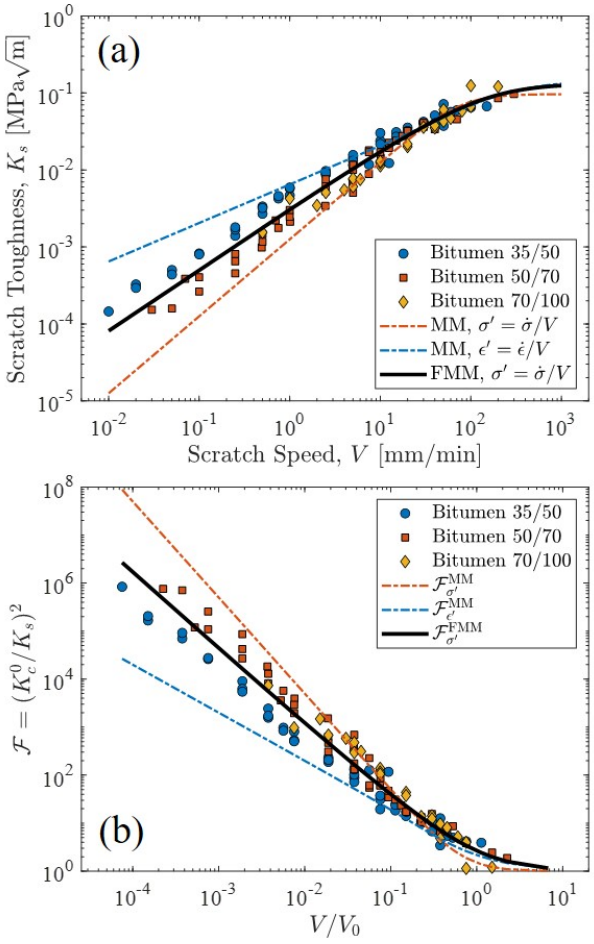

FIG. 2: (a) Scratch Toughness $K_s(V)$, and (b) Crack Speed Function $\mathcal{F}(V)$ vs. scratch speed V, for Bitumen samples of different grades. Displayed Models are fit to the experimental data: Maxwell Model for (i) constant stress rate (curve labeled MM, $\sigma' = \dot{\sigma}/V$ and $\mathcal{F}_{\sigma'}^{\text{MM}}$), (ii) constant strain rate (MM, $\epsilon' = \dot{\epsilon}/V$ and $\mathcal{F}_{\epsilon'}^{\text{MM}}$); and (iii) Fractional Maxwell Model for constant stress rate (FMM, $\sigma' = \dot{\sigma}/V$ and $\mathcal{F}_{\sigma'}^{\text{FMM}}$). The full listing of model parameters is provided in S.M. [28].

properties of our soft viscoelastic liquid (bitumen) does not extend to loading rate, $\dot{F}_v$, in contrast to reported scratch rate effects of 'hard' viscoelastic solids [19, 20].

We proceed by rationalizing our experimental observation through a first-order modeling of the different energy dissipation sources in the scratch test. Following earlier developments [18], we consider a fracture surface of length ℓ_c at a depth d ahead of the scratch probe [Fig. 1(c)]. Furthermore, we follow the scratch test setup and employ a moving coordinate system, $X_* = Vt - x$, with one subtle difference. We place the origin of the moving coordinate system, $X_* = 0$, at the crack front, which –given stationarity– moves with the same speed, V, as the scratch probe at $X_* = \ell_c$. The choice of the origin of the moving coordinate system is not neutral in view of separating the two different sources of energy dissipation, namely, fracture surface propagation and bulk viscous deformation. In fact, it allows us to write the change in potential energy in the form:

$$\frac{dE_{pot}}{dt} = V\frac{dE_{pot}}{dX_*} = -V\left(\mathcal{G}p + \int_\Omega \sigma_{ij}\frac{d\varepsilon^v_{ij}}{dX_*}d\Omega\right) \quad (2)$$

The first term on the r.h.s. of Eq. (2) represents the surface dissipation rate due to fracture, with $\mathcal{G} = -\partial E_{pot}/\partial\Gamma$ the energy release rate, which is the driving force of fracture surface creation $d\Gamma = -pdX_*$ (with p the probe perimeter), and which equals the fracture energy $\mathcal{G}^0_c$ in stationary fracture propagation; whereas the second term represents the volumetric viscous dissipation rate, with the stress tensor, σ_{ij}, being the driving force of viscous deformation in the dissipation rate density, $\sigma_{ij}\dot{\varepsilon}^v_{ij} = V\sigma_{ij}d\varepsilon^v_{ij}/dX_*$. With the origin of the moving coordinate system placed at the crack front, we can use classical surface integral expressions of the energy release rate, known as J-Integral [31, 32] to determine the driving force of the fracture process, $\mathcal{G}$, from [18, 21]:

$$\mathcal{G} = \frac{1}{p}\int_S(-\psi + \sigma_{xx}\epsilon_{xx})dS \quad (3)$$

where the surface integral taken over the free energy density, $\psi = \sigma^2_{xx}/(2E_0)$, and the stress-strain work density, $\sigma_{xx}\epsilon_{xx} = -F_T/A\epsilon_{xx}$ (with A the probe-material contact area projected onto the scratch direction; for details, see [21]), is carried out over the probe-material interface, S. That is, the strain ϵ_{xx}, which contains both an elastic and a viscous component, needs to be evaluated in the moving coordinate system, at $X_* = \ell_c$. This is a significant departure of our approach from earlier contributions [19, 20] affecting model input and output in three substantial ways: (i) Instead of strain rate $\dot{\varepsilon}$ relative to a fixed coordinate system, we use the spatial stress rate in the moving coordinate system, $\sigma' = \dot{\sigma}/V = d\sigma/dX_*$. Based on a simple dimensional argument, this stress rate is constant over the fracture length $X_* \in]0, \ell_c]$, i.e., $\sigma' = \sigma_0/(\tau V)H(X_*)$, with $\sigma_0 = -F_T/A = -K_s\sqrt{2p/A}$ the stress at the probe-material interface, τ the relaxation time of the viscoelastic liquid, and $H(X_*)$ the Heaviside function. (ii) Instead of time t, we integrate the viscoelastic rate equations in the moving coordinate system with respect to X_* to obtain the strain at the probe–material interface in excess of the rate-independent elastic deformation $\varepsilon_{xx}(\overline{X}_* = \ell_c/(\tau V)) = (\sigma_0/E_0)[1 + \int_0^{\ell_c/(\tau V)} E_0 J_v(\overline{X}_*)d\overline{X}_*]$, with $J_v(\overline{X}_*)$ the viscous creep compliance in function of the dimensionless spatial coordinate $\overline{X}_* = X_*/(\tau V)$; and (iii) substitution into the J-integral given in Eq. (3) provides an explicit means of evaluating the crack speed function $\mathcal{F}(V)$ from (see S.M. [28]):

$$\mathcal{G}_{\sigma'} = \mathcal{G}_s\mathcal{F}_{\sigma'}; \quad \mathcal{F}_{\sigma'} = 1 + \int_0^{V_0/V} E_0 J_v(\overline{X}_*)d\overline{X}_* \quad (4)$$

where $V_0 = \ell_c/\tau$. This stress-rate approach is significantly different from the strain-rate approach, in which the strain at the probe-material interface is evaluated from $\epsilon_{xx} = \epsilon'\ell_c$ (with $\epsilon' = \dot{\epsilon}/V$), and which involves the integral over the relaxation modulus, $E(\overline{X}_*)$, in the moving coordinate system (see S.M. [28]):

$$\mathcal{G}_{\epsilon'} = \mathcal{G}_s\mathcal{F}_{\epsilon'}; \quad \mathcal{F}_{\epsilon'} = \frac{2V_0/V}{\int_0^{V_0/V} E(\overline{X}_*)/E_0 d\overline{X}_*} - 1 \quad (5)$$

For purpose of illustration, consider a Maxwell Model (MM), a spring (stiffness E_0, elastic strain, $\epsilon - \epsilon^v$) in series with a dashpot (viscosity $\eta = E_0\tau$, viscous strain ϵ^v). We first transform the rate equation, $\sigma = E_0(\epsilon - \epsilon^v) = \eta\dot{\epsilon}^v$ into the moving coordinate system, $\dot{\epsilon}^v = V(d\epsilon^v/dX_*)$, and then evoke the correspondence principle of linear viscoelasticity [33] to take the Laplace transform w.r.t. X_*, $\hat{\sigma}(s_*) = s_*\hat{E}(s_*)\hat{\epsilon}(s_*)$; where $s_*\hat{E}(s_*) = E_0 V\tau s_*/(1 + V\tau s_*)$ is the s_*-multiplied relaxation modulus; respectively the inverse, the s_*-multiplied compliance function, $s_*\hat{J} = (s_*\hat{E})^{-1}$. Taking the inverse Laplace transform of respectively $\hat{E}(s_*)$ and $\hat{J}(s_*)$, provides the relaxation modulus, $E(\overline{X}_*) = E_0\exp(-\overline{X}_*)$, and the compliance function, $J(\overline{X}_*) = E_0^{-1} + J_v(\overline{X}_*)$, with $J_v(\overline{X}_*) = E_0^{-1}\overline{X}_*$ the viscous creep compliance that defines the deformation in excess of elastic deformation. From Eqs. (4) and (5) the crack speed functions for the Maxwell model are obtained:

$$\mathcal{F}^{\mathrm{MM}}_{\sigma'} = 1 + \frac{1}{2}\left(\frac{V_0}{V}\right)^2; \quad \mathcal{F}^{\mathrm{MM}}_{\epsilon'} = \frac{2V_0/V}{1 - \exp(-V_0/V)} - 1 \quad (6)$$

The predictive quality of the Maxwell model can be depicted from Fig. 2(a) (curves labeled 'MM σ'' and 'MM ϵ''). It is not surprising that a Maxwell model with a single relaxation time cannot capture the complex relaxation behavior of highly viscous suspensions such as bitumen with relaxation times that typically span orders of magnitude [7]. Indeed, while a single relaxation time, $\tau = \eta/E_0$, provides reasonable estimates for high scratch speeds (i.e., small relaxation times), both stress-rate and strain-rate approaches diverge at low scratch

speeds (i.e., large relaxation times). This shortcoming of the Maxwell model is well known from the investigation of rheological properties of soft viscoelastic solids and liquids. It brought about the application of fractional rate equations [34] to describe the large diversity of rate-dependent behavior of power-law materials (for a review, see [35]), including asphalt binders [36]. The extension to a Fractional Maxwell Model (FMM) is almost straightforward, when considering for the viscous (i.e., non-instantaneous) part of the deformation two springpot elements in series, described by the creep compliance, $J_v(\overline{X}_*) = E_0^{-1}[\overline{X}_*^{\alpha}/\Gamma(1+\alpha) + \overline{X}_*^{\beta}/\Gamma(1+\beta)]$, where Γ is the complete Gamma function, and $(\alpha, \beta) \in]0, 1]$ the fractional exponents, with the lower bound corresponding to a spring, and the upper bound to a linear dashpot [34]. While it could be (and has been) argued that fractional models, which include both elastic and viscous deformation, make it difficult to unambiguously evaluate the free energy density, ψ (for a discussion, see [37]), we use the fractional model here only for the description of non-instantaneous deformation. In contrast, the free energy density, $\psi = \sigma_0^2/2E_0$, and the elastic strain, $\epsilon_{xx} - \epsilon_v = \sigma_0/E_0$ are representative of the recoverable work under instantaneous loading, $V \to \infty$. The FMM thus permits the following expression of the crack speed function:

$$\mathcal{F}_{\sigma'}^{\mathrm{FMM}} = 1 + \frac{(V_0/V)^{1+\alpha}}{\Gamma(2+\alpha)} + \frac{(V_0/V)^{1+\beta}}{\Gamma(2+\beta)} \qquad (7)$$

The model thus derived has four adjustable parameters: The asymptotic scratch toughness, K_c^0; a reference speed, $V_0 = \ell_c/\tau$, which combines the fracture length, ℓ_c, and the characteristic relaxation time, τ; and the fractional exponents, α and β. While K_c^0 and $V_0 = \ell_c/\tau$ are related to the scratch-fracture test, the fractional exponents permit an independent experimental determination. We thus proceed as follows: In a first step we independently determine the fractional exponents from frequency sweep experiments in a cone-plate geometry connected to a stress-controlled rheometer (ARG2, TA instruments). The linear viscoelastic spectrum (Fig. 3), characterized by the frequency dependence of the storage and loss moduli, $G' = \mathrm{Re}(G^*)$ and $G'' = \mathrm{Im}(G^*)$ respectively, is fitted with a Fractional Maxwell Model. Specifically, the fractional exponents (α, β) are obtained by asymptotic matching between the energy-loss dominated regime at low frequencies ($G' < G'' \sim \omega^{\alpha}$) and the energy-storage dominated regime at high frequencies ($G'' < G' \sim \omega^{\beta}$), together with the characteristic relaxation time τ, which defines the cross-over between the two. (For sample preparation, experimental and fitting details, see S.M. [28], which cites Refs. [38–42]). In a second step, we use the fractional exponents to fit the remaining fracture related model parameters (V_0, K_c^0) using the analytical crack speed function displayed in Eq. (7). The predictive power of this two-step determination procedure shown in Figs. 2(a-b) provides strong evidence of the relevance of our scratch model to (i) quantitatively capture rate effects in the fracture response of viscoelastic liquids, and by doing so, (ii) allow the determination of the rate-independent fracture toughness of soft materials. That is, for bitumen, $K_c^0 = 0.126$ MPa$\sqrt{\mathrm{m}}$ with 95% confidence bounds $(0.066, 0.187)$ MPa$\sqrt{\mathrm{m}}$, reference speed $V_0 = 119.3$ $(4.225, 234.3)$ mm/min, and the fractional exponents $\alpha = 0.766$ $(0.404, 0.915)$, and $\beta = 0.110$ $(0.053, 0.253)$. We also obtain an estimate of the viscous fracture length ahead of the scratch probe, $\ell_c = V_0\tau = 410$ μm (for $\tau = 0.21 \pm 0,04$ s across samples, see [28]), which –not surprisingly– is commensurate with and controlled by the scratch depth [Fig. 1(d)].

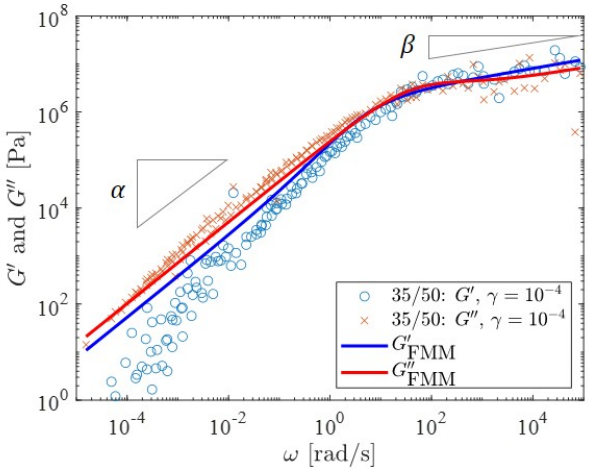

FIG. 3: Linear viscoelastic spectrum for a bitumen sample 35/50, i.e., storage and loss modulus, G' and G'', respectively, vs. frequency (ω). Data obtained at various temperatures between 5 and 85°C, and rescaled using the time-temperature superposition principle, using 25°C as a reference temperature. Continuous lines stand for the Fractional Maxwell Model (FMM) fit of the data matching the asymptotes at low and high frequencies, from which the fractional exponents α and β are derived. The full listing of model parameters for different Bitumen samples is provided in S.M. [28].

In summary, we have extended the realm of the scratch technique, well-entrenched for material characterization of 'hard' materials, to viscoelastic liquids, in which rate-dependent bulk viscous dissipation competes with instantaneous fracture energy dissipation for stored elastic (i.e., reversible) energy. Compared to other techniques, the advantage of the proposed instrumented scratch method and model is its in-built control, both experimentally and theoretically, of the stationarity of the fracture process. This permits us to discriminate, with high fidelity, between rate effects and rate-independent fracture properties of soft materials, at a length scale controlled by the scratch depth.

From a more practical point of view, our investigation provides the first fracture toughness values of bitumen,

the binding phase of asphalt, a core material of our built infrastructure. The found value of $K_c^0 = 0.1$ MPa$\sqrt{\text{m}}$ is by -at least- one order smaller than scratch toughness values of other colloidal infrastructure materials such as cement paste [43, 44], which may explain the high deterioration rate of asphalt materials and our pavement networks worldwide, in urgent need of materials' innovation.

Research carried out by the joint MIT-CNRS-AMU research unit (2012–2020), enabled by MIT's Energy Initiative, with sponsorship provided by Ferrovial S.A., and the collaboration of its subsidiary company, Ditecpesa, Spain.

* Electronic address: CorrespondingAuthor:ulm@mit.edu

[1] R. Long and C.-Y. Hui, *Soft Matter* **12**, 8068–8086 (2016).
[2] E.B. Caldona, A. Christopher, C.D. Leon, B.B. Pajarito and R.C. Advincula, *Polym. Rev.* **57**, 311 (2017).
[3] C. Creton, and M. Ciccotti, *Rep. Prog. Phys* **79**, 046601 (2016).
[4] J.R. Gladden and A. Belmonte, *Phys. Rev. Lett.* **98**, 224501 (2007).
[5] H. Tabuteau, S. Mora, G. Porte, M. Abkarian and C. Ligoure, *Phys. Rev. Lett.* **102**, 155501 (2009).
[6] C. Ligoure and S. Mora, *Rheol. Acta* **52**, 91 (2013).
[7] E. Behzadfar, S.G. Hatzikiriakos, *Fuel* **108**, 391 (2013).
[8] O. Coussy, *Int. J. Eng. Sci.* **25**, 609 (1987).
[9] T. Goldman Boué, R. Harpaz, J. Fineberga and E. Bouchbinder, *Soft Matter* **11**, 3812 (2015).
[10] J. Guo A.T. Zehnder, C. Creton and C.-Y. Hui, *Soft Matter* **16**, 6163 (2020).
[11] A.Y. Malkin and C.J.S. Petrie, *J. Rheol.* **41**, 1 (1997).
[12] R.S. Rivlin and A.G. Thomas, *J. Polym. Sci.* **10**, 291 (1953).
[13] H.W. Greensmith, *J. Appl. Polym* **7**, 993 (1963).
[14] A.N. Gent, *Langmuir* **12**, 4492 (1996).
[15] T. Baumberger, C. Caroli and D. Martina, *Nat. Mat.* **5**, 552 (2006).
[16] S. Kundu and A.J. Crosby, *Soft Matter* **5**, 3963 (2009).
[17] S. Chockalingam, C. Roth, T. Henzel, T. Cohen, *J. Mech. Phys. Solids* **146**, 104172 (2021).
[18] A.-T. Akono, P.M. Reiss and F.-J. Ulm, *Phys. Rev. Lett.* **106**, 204302 (2011).
[19] A.-T. Akono and F.-J. Ulm, *J. Nanomech. Micromech.* **7**, 04017009 (2017).
[20] P. Kabir, F.–J. Ulm and A.–T. Akono, *Acta Geotech.* **12**, 1207 (2017).
[21] A.-T. Akono and F.-J. Ulm, *J. Mech. Phys. Solids* **60**, 379 (2012).
[22] A.-T. Akono, F.-J. Ulm and Z.P. Bažant, *Eng. Fract. Mech.* **119**, 21 (2014).
[23] D. Lesueur, *Adv. Colloid Interface Sci.* **145**, 42 (2009).
[24] ASTM D946 / D946M-20, Standard Specification for Penetration-Graded Asphalt Binder for Use in Pavement Construction, *ASTM International*, West Conshohocken, PA (2020).
[25] L.B. Freund, Dynamic Fracture Mechanics, Cambridge University Press, (1990, online 2009).
[26] D. Bonamy and E. Bouchaud, Failure of heterogeneous materials: A dynamic phase transition?, *Physics Reports* **498**, 1 (2011).
[27] G. Irwin, 1958. In: S. Flugge, S. (Ed.), *Handbuch der Physik*. Springer-Verlag, Berlin, (1958).
[28] Supplemental Material, which provides detailed information about (*i*) the scratch test setup and calibration, (*ii*) derivation of the scratch-fracture model in a moving coordinate system, and (*iii*) the rheological tests and analysis of the results. (http-address to be added).
[29] A.-T. Akono, N.X. Randall and F.-J. Ulm, *J. Mater. Res.* **27**, 485 (2012).
[30] A.-T. Akono and F.-J. Ulm, *Wear* **313**, 117 (2014).
[31] G.P. Cherepanov, *Appl. Math. Mech.* **31**, 503 (1967).
[32] J.R. Rice, *J. Appl. Mech.* **35**, 379 (1968).
[33] R.M. Christensen, *Theory of Viscoelasticity*, 2nd Ed., Academic Press, New York (2003).
[34] H. Schiessel, R. Metzler, A. Blumen and T.F. Nonnemacher, *J. Phys. A: Math. Gen.* **28**, 6567 (1995).
[35] A. Bonfanti, J.L. Kaplan, G. Charras and A. Kabla, *Soft Matter* **16** 6002 (2020).
[36] W. Cao, *J. Rheol.* **64**, 1439 (2020).
[37] L. Deseri, M. Di Paola, and M.Zingales, *Int. J. Sol. and Struct.* **51**, 3156 (2014).
[38] A. Jaishankar and G.H. McKinley, *Proc. R. Soc. A* **469**, 20120284 (2013).
[39] A. Jaishankar, Doctoral dissertation, Massachusetts Institute of Technology, (2011).
[40] B. Keshavarz, T. Divoux, S. Manneville and G.H. McKinley, *ACS Macro Letters* **6**, 663 (2017).
[41] J. Dealy and D. Plazek, *Rheol. Bull.* **78**(2), 16 (2009).
[42] M.L. Williams, R.F. Landel and J.D. Ferry, *J. Am. Chem. Soc.* **77**(14), 3701.
[43] C.G. Hoover and F.-J. Ulm, *Cem. Concr. Res.* **75**, 42 (2015).
[44] K.J. Krakowiak, J.J. Thomas, S. Musso, S. James, A.-T. Akono and F.-J. Ulm, *Cem. Concr. Res.* **67**, 103 (2015).